

Research Article

Open Access



First-principles study on crystal structures and superconductivity of ternary metal hydride La-Sr-H under high pressure

Ling Chen, Qiwen Jiang, Zihan Zhang, Zhengtao Liu, Zihao Huo, Hao Ma, Shumin Guo, Shouwen Yang, Defang Duan

Key Laboratory of Material Simulation Methods & Software of Ministry of Education, State Key Laboratory of Superhard Materials, College of Physics, Jilin University, Changchun 130012, Jilin, China.

Correspondence to: Assoc Prof. Shouwen Yang, Key Laboratory of Material Simulation Methods & Software of Ministry of Education, State Key Laboratory of Superhard Materials, College of Physics, Jilin University, 2699 Qianjin St., Changchun 130012, Jilin, China. E-mail: yangsw@jlu.edu.cn; Prof. Defang Duan, Key Laboratory of Material Simulation Methods & Software of Ministry of Education, State Key Laboratory of Superhard Materials, College of Physics, Jilin University, 2699 Qianjin St., Changchun 130012, Jilin, China. E-mail: duandf@jlu.edu.cn

How to cite this article: Chen, L.; Jiang, Q.; Zhang, Z.; Liu, Z.; Huo, Z.; Ma, H.; Guo, S.; Yang, S.; Duan, D. First-principles study on crystal structures and superconductivity of ternary metal hydride La-Sr-H under high pressure. *Microstructures* 2025, 5, 2025042. <https://dx.doi.org/10.20517/microstructures.2024.21>

Received: 29 Feb 2024 **First Decision:** 26 Apr 2024 **Revised:** 20 May 2024 **Accepted:** 24 May 2024 **Published:** 17 Apr 2025

Academic Editor: Liangzhi Kou **Copy Editor:** Fangling Lan **Production Editor:** Fangling Lan

Abstract

The discovery of cage hydrides $(Y,Ca)H_6$, $(La,Ce)H_9$, and $(La,Y)H_{10}$ indicates the appeal of ternary hydrides as contenders for high-temperature superconductors. Herein, we systematically studied a La-Sr-H system and predicted interesting stable and metastable hydrides at 200 GPa by first-principles calculations. The results revealed that $LaSrH_{21}$ has a high superconducting transition temperature (T_c) of 211 K at 200 GPa, mainly attributed to its unique H_{12} rings. $LaSrH_{12}$, $LaSr_2H_{18}$, and $LaSr_3H_{24}$ contain distorted H_{24} cages and exhibit high T_c values of 160, 167, and 169 K, respectively. Notably, $LaSrH_{12}$ maintained dynamic stability down to 30 GPa, which is extremely low for H_{24} cage hydrides. In addition, the T_c s of $LaSrH_{12}$ increased at a rate of 0.43 K/GPa with the increase in pressure. Further analysis revealed that the positive pressure-dependent T_c was mainly due to the softening of the low-frequency phonon modes and Lifshitz transition. Our work will guide the study of ternary rare- and alkaline-earth hydrides.

Keywords: High pressure, first-principles calculations, hydrides, superconductivity



© The Author(s) 2025. **Open Access** This article is licensed under a Creative Commons Attribution 4.0 International License (<https://creativecommons.org/licenses/by/4.0/>), which permits unrestricted use, sharing, adaptation, distribution and reproduction in any medium or format, for any purpose, even commercially, as long as you give appropriate credit to the original author(s) and the source, provide a link to the Creative Commons license, and indicate if changes were made.



INTRODUCTION

The Bardeen-Cooper-Schrieffer (BCS) theory suggests that high Debye temperature and pronounced electron-phonon coupling (EPC) of metallic hydrogen make it a promising candidate for high-temperature superconductivity^[1-3]. Pressure is an important thermodynamic parameter that can shorten atomic distance and regulate the electronic structure of materials^[4,5]. It is well known that it can transform the insulating hydrogen to a metallic state. However, a pressure of at least 500 GPa is required for the atomic metallic phase of hydrogen^[6,7], which is not feasible under the current experimental conditions. In 2004, Ashcroft proposed the concept of chemical precompression^[8] to attain high-temperature superconductivity at lower pressures^[9]. Based on this principle, earlier studies could only focus on naturally occurring hydrides such as AlH_3 ^[10] and SiH_4 ^[11]. Although these studies revealed the need for effective reductions in pressure to enter the superconducting state, the superconducting transition temperatures (T_c) failed to reach satisfactory levels. With the development of crystal structure prediction^[12-19], numerous nonstoichiometric superhydrides with high T_c have been theoretically predicted, and some have been experimentally synthesized^[20-32]. Hydrogen-based superconductors H_3S ^[20-23] and LaH_{10} ^[24-28] are widely concerned. H_3S is a covalent hydride in which S atoms form a body-centered cubic lattice, with H atoms symmetrically positioned between them, which is theoretically predicted to have a high T_c of 191-204 K at 200 GPa, and then confirmed by experimental with T_c of 203 K above 155 GPa. LaH_{10} serves as a representative cage hydride, in which weak covalent bonds between H atoms form hydrogen cages, and the La atoms at the center of the hydrogen cages provide electrons to stabilize the hydrogen cages. The theoretically predicted T_c of LaH_{10} is about 288 K at 200 GPa^[24,25] and the experimentally measured T_c is 250-260 K at 180-200 GPa^[26-28]. The difference of T_c and stable pressure between experiment measurement and theoretical prediction has been well explained by anharmonic effect of hydrogen atoms^[33,34]. The discovery of these two hydrides prompted a rush of research on hydrogen-rich superconductors under high pressure^[32].

Thus far, the superconductivities of almost all binary hydrides have been systematically predicted, and most of them, such as CaH_6 ^[31] (215 K at 172 GPa), CeH_9 ^[35] (57 K at 85 GPa), and ThH_{10} ^[36] (159-161 K at 170-175 GPa), have been experimentally synthesized. However, 90% of the hydrides fell below the liquid ammonia refrigeration range (195 K). Ternary hydrides possess more complex morphological combinations than binary hydrides, suggesting their possible novel properties. Sun *et al.* theoretically predicted that $\text{Li}_2\text{MgH}_{16}$ ^[37] can reach a high T_c of 473 K at 250 GPa and provides a new strategy toward improving the superconductivity of binary hydrides by incorporating metal elements into binary hydrides rich in H_2 or H_3 molecular units. LaBeH_8 with a Be-H alloy was predicted to maintain thermodynamical stability above 98 GPa and remain dynamically stable at 20 GPa with a high T_c of 185 K^[38]. Recently, LaBeH_8 was successfully synthesized in a pressure range of 110-130 GPa, and its T_c can reach 110 K at 80 GPa^[39]. The successful experimental synthesis in the theoretically predicted pressure range demonstrates the foresight of theoretical prediction. Another research direction for ternary hydrides involves mixing other metal elements with the original high T_c hydrides, namely CaH_6 , YH_9 ^[40], and LaH_{10} , to obtain caged hydrides: $(\text{Y,Ca})\text{H}_6$ ^[41-43], $(\text{La,Ce})\text{H}_9$ ^[44,45], and $(\text{La,Y})\text{H}_{10}$ ^[46]. $(\text{Y,Ca})\text{H}_6$ was theoretically predicted to possess good superconducting properties with a T_c above 200 K. In addition, Ma *et al.* used high-throughput calculations to design a series of $\text{Pm}\bar{3}m$ phase ternary hydrides $(\text{M,X})\text{H}_6$ and proposed an AE model (a predictive tool for superconducting critical temperatures in cage-like hydrides, based on Average Electron Localization Function values at the center of all H-H bonds and contribution of hydrogen to Density of States at the Fermi level) to estimate the T_c of the clathrate hydrides^[47]. $(\text{La,Ce})\text{H}_9$ ^[44,45] was successfully synthesized experimentally, although it contained a LaH_9 unit, which is unstable in the La-H system. In addition, in synthetically experimentally obtained $(\text{La,Y})\text{H}_{10}$ ^[46], the Y atoms and their neighboring H atoms formed Y@H_{32} fragments, which contained a locally distorted H-cage specific to $\text{Fm}\bar{3}m\text{-YH}_{10}$.

In previous studies of binary hydrides, strontium (Sr)^[48–52] and lanthanum (La) hydrides have attracted considerable attention because of their unique crystal structures and remarkable superconducting properties. Sr hydrides include several compounds with a high hydrogen content. SrH₆, with linear and bent H₃ units, transforms into spiral polymer H chains at 250 GPa^[53]; SrH₁₀ possesses a graphene-like H-layer at 300 GPa, and SrH₂₂, which is the metal hydride with the highest hydrogen content discovered thus far, contains H₂ units at 146 GPa. The rare-earth metal La contains more valence electrons than the alkaline-earth Sr and can transfer more electrons to hydrogen atoms. This condition enables H to obtain sufficient electrons to fill the antibonding σ^* orbitals, which weakens the H-H bonds in the H₂ and H₃ units. Therefore, introducing La into binary Sr-H systems can form new ternary hydrides, which may exhibit novel properties, such as high T_c under high pressure.

In this work, we determined the crystal structures and superconducting properties of a La-Sr-H system at 200 GPa and observed the thermodynamically stable LaSrH₄*P3m1*, LaSrH₄*P6/mmm*, LaSrH₁₂*R3m*, and LaSr₃H₂₄*R3m* and metastable LaSr₂H₁₈*C2/m* and LaSrH₂₁*Cm*. They all exhibited good superconducting properties, except for LaSrH and LaSrH₄, which had low hydrogen content. The metastable structure of LaSrH₂₁ had a high T_c of 211 K at 200 GPa, in which H atoms around La were arranged in an H₁₂ ring layer. LaSrH₁₂ is predicted to possess a high T_c of 160 K at 200 GPa and remain dynamically stable down to 30 GPa. LaSr₂H₁₈ and LaSr₃H₂₄ achieved high T_c of 164 and 169 K at 200 GPa, respectively.

COMPUTATIONAL DETAILS

The structure of the La-Sr-H system at 200 GPa was searched using the USPEX^[16,18] (Universal Structure Predictor: Evolutionary Xtallography) structure prediction method coupled with ab initio geometry optimizations implemented in Vienna ab initio simulation packages (VASP) code^[54]. During the variable-component search, the maximum number of atoms was set to 28. The number of generations was set to 30, in which the first generation contained 200 individuals and each subsequent generation involved 50 individuals. After the structural search, we evaluated the thermodynamic and structural stability of the system using the convex hull method and phonon calculations. The crystal structure was optimized using the VASP code, which was used to calculate the electronic properties. We selected Perdew-Burke-Ernzerhof (PBE)^[55] of the generalized gradient approximation (GGA)^[56] as the exchange-correlation function. In addition, the all-electron projector-augmented wave method^[57] was used to describe ion-electron interactions. To ensure that the enthalpy converged to less than 1 meV/atom, we set the cutoff energy to 850 eV and adopted Monkhorst-Pack k meshes with a grid spacing of $2\pi \times 0.03 \text{ \AA}^{-1}$. The crystal orbital Hamiltonian population (COHP) and its integral were calculated using the LOBSTER^[58] code.

Phonon calculations were performed using the supercell method implemented in the PHONOPY^[59] code, which was also used for zero-point energy (ZPE) corrections. The EPC and superconducting properties were calculated using density functional perturbation theory, as implemented in the Quantum-ESPRESSO code^[59,60]. Ultrasoft pseudopotential^[61] and GGA-PBE were used with a kinetic energy cutoff of 85 Ry and a charge density cutoff of 850 Ry. During EPC calculation, the numbers of q- and k-points were as follows: $3 \times 5 \times 3$ and $12 \times 20 \times 12$ for LaSrH₄*P3m1*, $5 \times 5 \times 3$ and $20 \times 20 \times 12$ for LaSrH₄*P6/mmm*, $3 \times 4 \times 3$ and $12 \times 16 \times 12$ for LaSrH₈*Pmma*, $5 \times 5 \times 5$ and $20 \times 20 \times 20$ for LaSrH₁₂*R3m*, $5 \times 5 \times 3$ and $20 \times 20 \times 12$ for LaSr₂H₁₈*C2/m* and LaSrH₂₁*Cm*, and $4 \times 4 \times 4$ and $16 \times 16 \times 16$ for LaSr₃H₂₄*R3m*.

Allen-Dynes formula was used to calculate the T_c of La-Sr-H compounds^[62]:

$$T_c = \frac{f_1 f_2 \omega_{log}}{1.2} \exp \left[-\frac{1.04 + 1.04\lambda}{\lambda - \mu^* - 0.63\lambda\mu^*} \right] \quad (1)$$

where μ^* refers to the Coulomb pseudopotential; λ and ω_{log} represent the EPC constant and logarithmic average frequency, respectively.

$$\lambda = \int_0^{\omega_{max}} \frac{2\alpha^2 F(\omega)}{\omega} d\omega \quad (2)$$

$$\omega_{log} = \exp \left(\frac{2}{\lambda} \int_0^{\omega_{max}} \frac{2\alpha^2 F(\omega) \ln \omega}{\omega} d\omega \right) \quad (3)$$

Here, $\alpha^2 F(\omega)$ is an Eliashberg function.

when $\lambda < 1.5$, $f_1 f_2 = 1$. Meanwhile, when $\lambda > 1.5$, the f_1, f_2 can be calculated as follows:

$$f_1 = \sqrt[3]{1 + \left(\frac{\lambda}{2.46(1 + 3.8\mu^*)} \right)^{\frac{3}{2}}} \quad (4)$$

$$f_2 = 1 + \frac{\left(\frac{\bar{\omega}_2}{\omega_{log}} - 1 \right) \lambda^2}{\lambda^2 + \left[1.82(1 + 6.3\mu^*) \frac{\bar{\omega}_2}{\omega_{log}} \right]^2} \quad (5)$$

where $\bar{\omega}_2$ is mean square frequency.

RESULTS AND DISCUSSIONS

A structural search of $\text{La}_x\text{Sr}_y\text{H}_z$ ($x = 1-3$, $y = 1-3$, $z = 1-24$) was performed within 60,000 structures at 200 GPa, and a ternary convex hull was constructed to determine the thermodynamic stability of the predicted ternary hydrides. Because ZPE is important for hydrogen-rich compounds, we constructed a ternary convex hull with it [Figure 1]. We located LaSrH , LaSrH_4 , LaSrH_{12} , and $\text{LaSr}_3\text{H}_{24}$ on the convex hull at 200 GPa, indicating that they are thermodynamically stable and do not decompose into other lower-energy phases. Moreover, LaSrH_8 , $\text{LaSr}_2\text{H}_{18}$, and LaSrH_{21} deviated by less than 20 meV/atom from the convex hull, suggesting that they are thermodynamically metastable. This finding did not preclude them from experimental synthesis. Many theoretically predicted metastable compounds have been successfully synthesized. Scholars have assumed that compounds with formation enthalpies of less than 50 meV/atom can be synthesized^[63,64]. Figure 2 shows the crystal structures of our predicted ternary hydrides, and Supplementary Table 1 in the Supplementary Materials lists their structural information.

Compounds LaSrH and LaSrH_4 were structurally stable with $P\bar{3}m1$ and $P6/mmm$, respectively. However, LaSrH and LaSrH_4 did not exhibit superconductivity, which is not discussed in the following text. The predicted metastable LaSrH_8 adopted the $Pmma$ space group. Figure 3 shows the calculated electronic and phonon structures of the LaSrH_8 . The compound exhibited metallic character and a total density of states (DOS) of 11.48 states/spin/Ry/f.u. at the Fermi level N_{EF} . Although LaSrH_8 achieved a high DOS value at the Fermi level, the calculated T_c was only 71 K [Table 1], close to the liquid-nitrogen temperature. This result was mainly due to the electronic DOS at the Fermi level being mainly contributed by the f-state electrons of La atoms and the proportion of H DOS at the Fermi level only 28.3%, which adversely affected the superconductivity^[65].

Table 1. Superconducting parameters of La-Sr-H system compounds

Phase	Pressure (GPa)	N_{Ef} (states/spin/Ry/f.u.)	ω_{log} (K)	λ	T_c (K)
LaSrH ₈ - <i>Pmma</i>	200	11.48	933.2	1.00	60-71
LaSrH ₁₂ - <i>R3m</i>	30	5.39	659.5	1.39	80-90
LaSrH ₁₂ - <i>R3m</i>	50	5.14	854.0	1.21	84-95
LaSrH ₁₂ - <i>R3m</i>	100	4.84	1,002.8	1.25	104-117
LaSrH ₁₂ - <i>R3m</i>	150	4.99	944.5	1.53	133-146
LaSrH ₁₂ - <i>R3m</i>	200	5.55	859.3	1.70	146-160
LaSr ₂ H ₁₈ - <i>C2/m</i>	200	8.27	921.6	1.52	152-167
LaSr ₃ H ₂₄ - <i>R3m</i>	200	11.99	1,168.2	1.25	148-169
LaSrH ₂₁ - <i>Cm</i>	200	7.11	892.1	2.11	196-211

T_c was calculated through the self-consistent solution of the Eliashberg equation with $\mu^* = 0.1$ and 0.13.

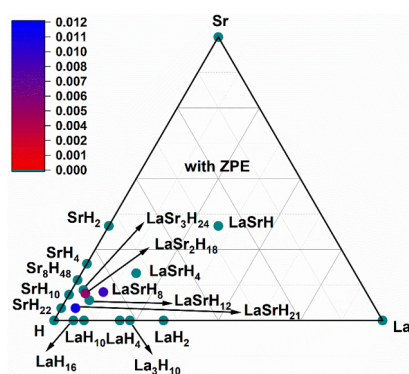


Figure 1. Ternary-phase diagram of the La-Sr-H system at 200 GPa with ZPE. Dark cyan dots represent stable structures, and other colored dots denote metastable structures.

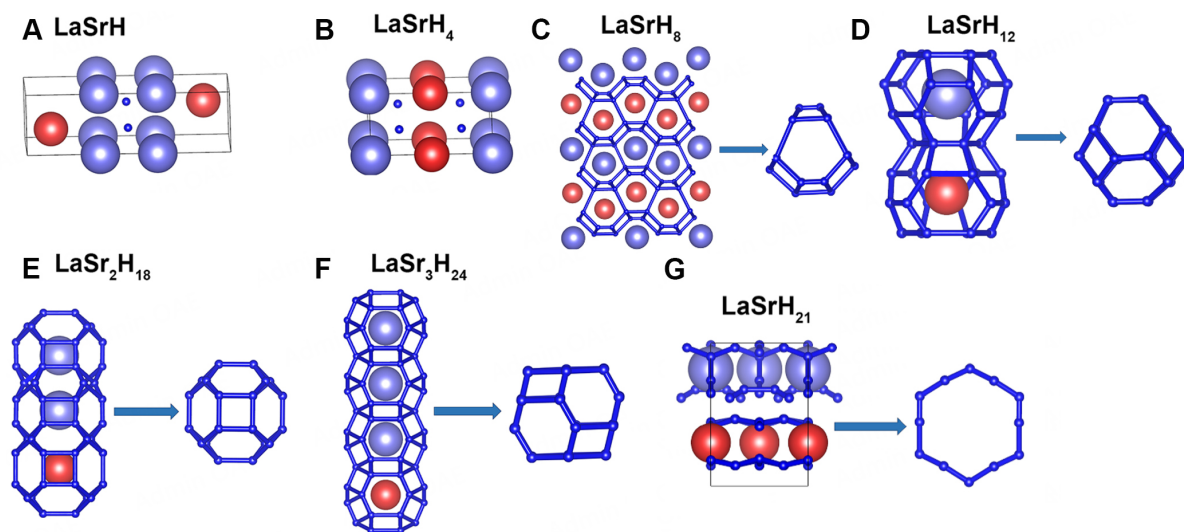


Figure 2. Crystal structures of the La-Sr-H system at 200 GPa. (A) LaSrH-*P3m1*, (B) LaSrH₄-*P6/mmm*, (C) LaSrH₈-*Pmma*, (D) LaSrH₁₂-*R3m*, (E) LaSr₂H₁₈-*C2/m*, (F) LaSr₃H₂₄-*R3m*, and (G) LaSrH₂₁-*Cm*. Red, gray-violet, and dark-blue balls represent La, Sr, and H atoms, respectively. The bonds between H₂ and H₃ units are represented as black dashed lines.

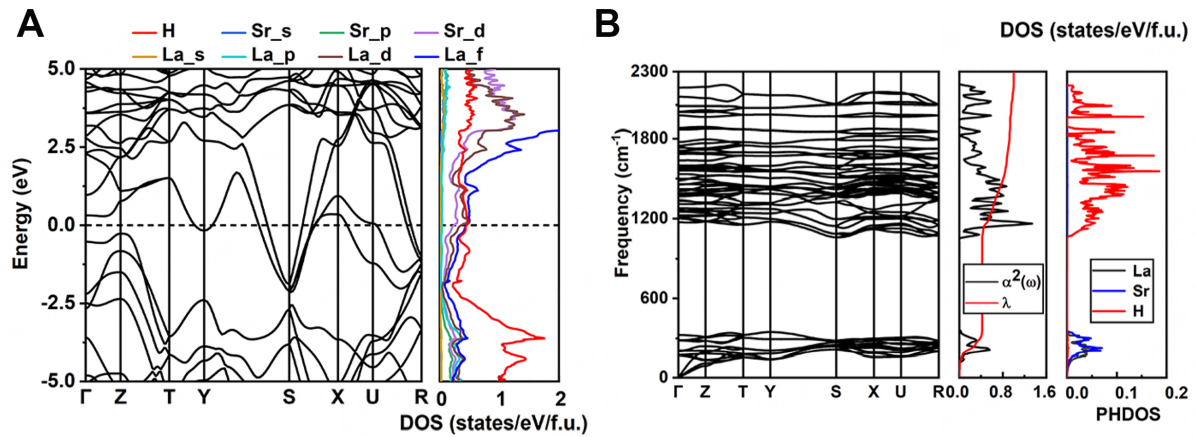


Figure 3. (A) Electronic band structures and projected DOS (PDOS) and (B) calculated phonon dispersion curves, Eliashberg spectral function $\alpha^2F(\omega)$ with electron-phonon integral $\lambda(\omega)$, and projected phonon DOS (PHDOS) for LaSrH₈-Pmma 200 GPa.

We also discovered an interesting metastable compound, LaSrH₂₁, with a layered structure and *Cm* symmetry. The layered structure containing La atoms was stacked in an ABA fashion, in which the A layer consisted of wrinkled H₁₂ rings, and the B layer comprised La atoms located below the center of the H₁₂ ring [Figure 2G]. The H₁₂ ring contained four different H-H bonds with lengths of 0.94, 1.04, 1.10, and 1.20 Å at 200 GPa, longer than the H-H bond length (~0.8 Å) in the H₂ molecular units of SrH₂₂. This result was due to the electrons obtained by hydrogen occupying the antibonding orbitals, which weakened the interactions between the hydrogen atoms and increased the bond length. In order to investigate the H-H bonding character in more detail, we calculated the electron localization function (ELF) and COHP of H₁₂ rings, as shown in Figure 4. As provided in Figure 4A, the ELF values of H atoms equal 0.6–0.8 indicating covalent bonds among H atoms. In Figure 4B, the left sides with negative values represent bonding states, and the right sides are antibonding states. The integrated COHP (ICOHP) up to the Fermi level represents the bonding interactions between H atoms; larger negative values represent stronger H-H bonds. The ICOHP values of those H-H distances such as 0.94, 1.04, 1.10, and 1.20 Å are -2.45, -1.62, -1.64 and -0.85 eV, respectively, indicating this unique H₁₂ ring was connected by weak covalent interactions. Furthermore, the band structures (left panel) and PDOS (right panel) of LaSrH₂₁ were calculated [Figure 5A]. The conduction and valence bands overlapped near the Fermi level, implying the metallic nature of this structure. The total DOS at the Fermi level is 7.11 states/spin/Ry/f.u., higher than that of LaSrH₁₂. However, the DOS value of H atoms at the Fermi level constitutes the main contribution with a value of 61.9%, higher than that of other structures (28.3% in LaSrH₈, 50.5% in LaSr₂H₁₈ and 48.7% in LaSr₃H₂₄). This phenomenon is beneficial for superconductivity. Figure 5B presents the Eliashberg spectral function $\alpha^2F(\omega)$ and electron-phonon integral $\lambda(\omega)$ at 200 GPa which is the critical pressure for dynamic stability. The medium-frequency H vibrational mode (500–2,500 cm⁻¹) contributed 71.9% of the EPC. From the PHDOS of LaSrH₂₁, the H₁₂ ring played a dominant role in the EPC. The calculated *T_c* of LaSrH₂₁ was 196–211 K at 200 GPa, which was attributed to the unique H₁₂ ring.

We also observed a series of hexahydrides (LaSrH₁₂, LaSr₂H₁₈, and LaSr₃H₂₄) with *R3m*, *C2/m*, and *R3m* symmetries, respectively. The crystal structures of these compounds are similar to that of typical CaH₆, which contains distorted H₂₄ cages with La or Sr as guest atoms filling the clathrate cavities, which provide electrons for the stabilization of the hydrogen cage [Figure 2D–F]. Each H₂₄ cage comprised eight hexagons and six quadrangles. Similar structures indicate the resemblance of the electronic and superconducting properties of hexahydrides. The results show that these hexahydrides are metallic and that hydrogen atoms contributed substantially to the DOS of the Fermi level [Figures 6 and 7]. The calculated *T_c*s for LaSrH₁₂,

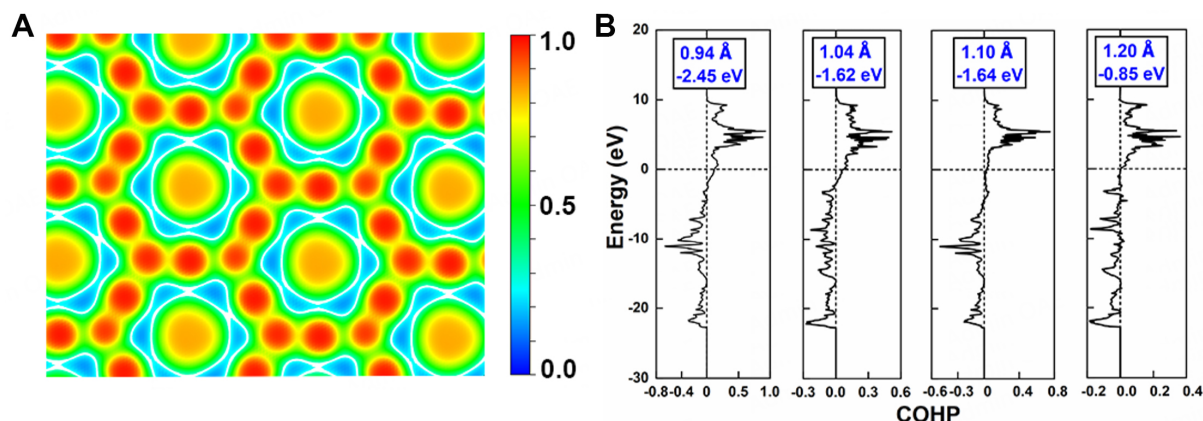


Figure 4. (A) ELF of LaSrH₂₁-Cm at 200 GPa of H₁₂ rings and (B) the COHP of four types of H-H bonds in H₁₂ rings for LaSrH₂₁-Cm at 200 GPa.

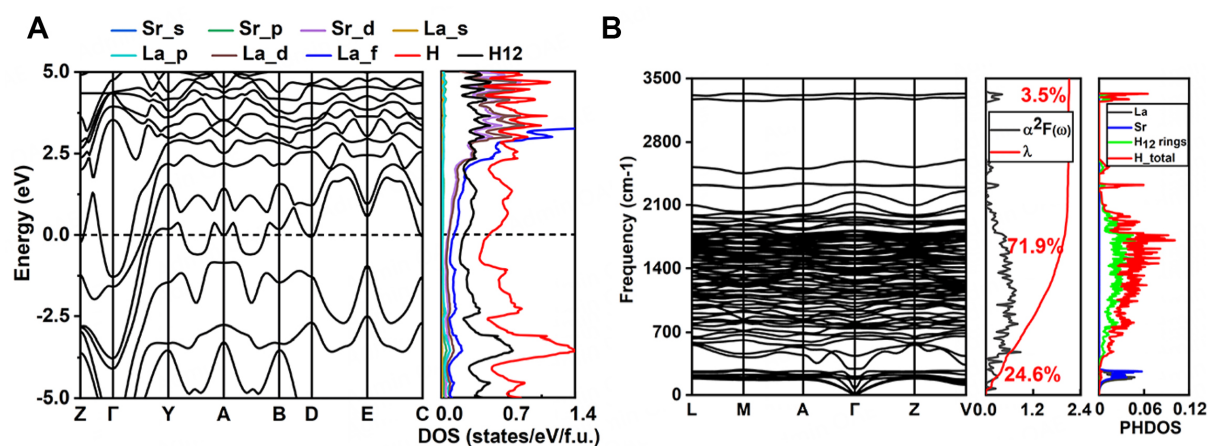


Figure 5. (A) Electronic band structures and PDOS and (B) calculated phonon dispersions, Eliashberg spectral function $\alpha^2F(\omega)$, electron-phonon integral $\lambda(\omega)$, and projected PHDOS for LaSrH₂₁-Cm at 200 GPa.

LaSr₂H₁₈ and LaSr₃H₂₄ were similar, with values of 160, 167, and 169 K, respectively, at 200 GPa, respectively [Table 1]. The difference is that LaSrH₁₂ could maintain its dynamic stability down to 30 GPa [Supplementary Figure 1], which was much lower than the dynamic stable critical pressure of YCaH₁₂-*Pm3̄m* (150 GPa)^[42], whereas LaSr₂H₁₈ and LaSr₃H₂₄ were only dynamically stable at 200 GPa [Figure 8]. Thus, we aimed to conduct a detailed investigation of the crystal structure, electronic properties and superconductivity of LaSrH₁₂ as a function of pressure.

The crystal structure of LaSrH₁₂ at 50 GPa is depicted in Figure 9A. We found half of the H atoms existed in the form of H₂ units. The H-H distance in H₂ units is 0.89 Å at 50 GPa, which elongates with pressure. At 200 GPa, it extends to 1.04 Å, much longer than the typical H-H bond length of 0.74 Å in pure solid hydrogen. Besides, we calculated its ELF map and COHP to study the H-H bonding character in detail. As shown in Figure 9B, the ELF and negative ICOHP values between H-H in H₂ units are 1.0 and 3.12 eV, respectively, indicating strong covalent bonds. The ELF and negative ICOHP values were about 0.8 and 2.08 eV at 200 GPa, respectively, which declined with the pressure increase. The variation trend of the nearest neighbor hydrogen distance and ICOHP value with increased pressure was shown in Figure 9C. The H-H distance in H₂ unit increases with pressure, and in the meantime, the negative ICOHP value

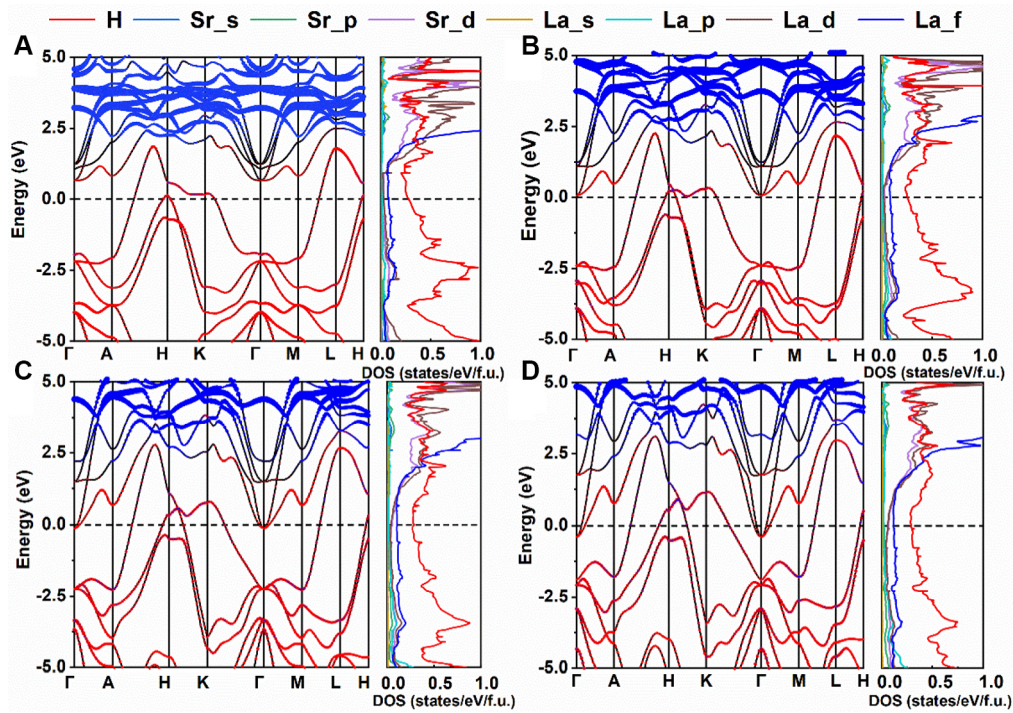


Figure 6. Electronic band structures and PDOS of LaSrH₁₂-R_{3m} at (A) 50, (B) 100, (C) 150, and (D) 200 GPa. The sizes of circles in the band structures denote the contributions of H atoms and the f orbital of La atoms. The red and blue dots represent H and La atoms, respectively.

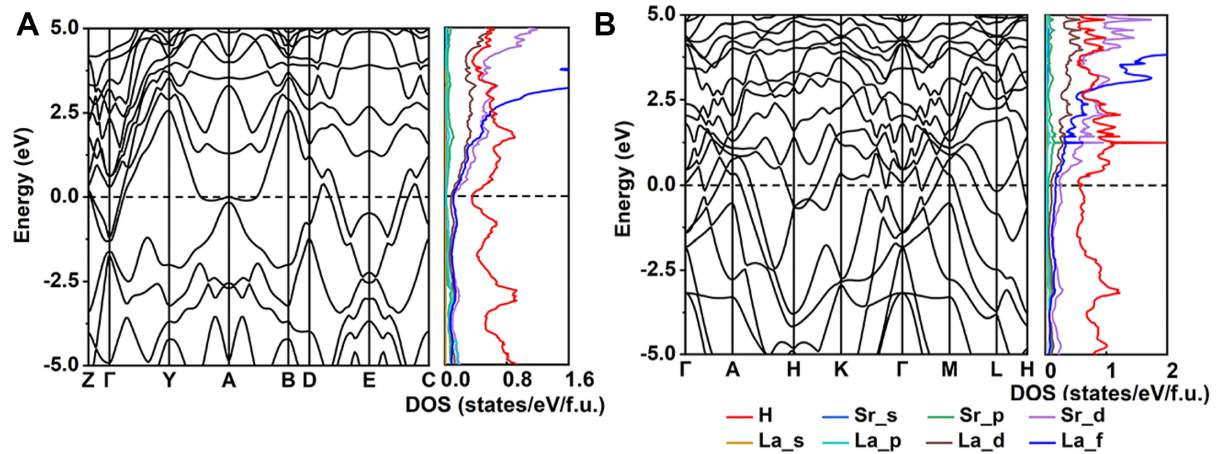


Figure 7. Calculated electronic band structures and PDOS of (A) LaSr₂H₁₈-C_{2/m} and (B) LaSr₃H₂₄-R_{3m} at 200 GPa.

diminished, indicating a weakening interaction between H atoms in H₂ units as pressure rises. This phenomenon is beneficial for improving superconductivity.

To examine the electronic properties of LaSrH₁₂ with increasing pressure, its electronic structures were calculated at 50, 100, 150, and 200 GPa [Figure 6]. As the pressure rose to 100 GPa, the lowest conduction band at the Γ point gradually descended but did not exceed the Fermi energy. In addition, the valence band located on the Fermi surface at the H-point moved upward, which caused the total electronic DOS at the

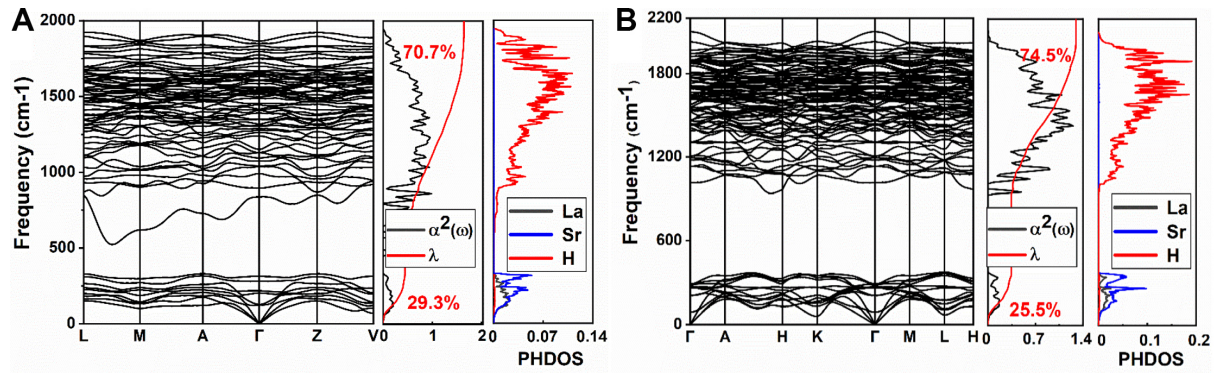


Figure 8. Phonon band structures, Eliashberg spectral function $\alpha^2F(\omega)$ with electron-phonon integral $\lambda(\omega)$, and projected PHDOS of (A) LaSr₂H₁₈-C2/m and (B) LaSr₃H₂₄-R3m at 200 GPa.

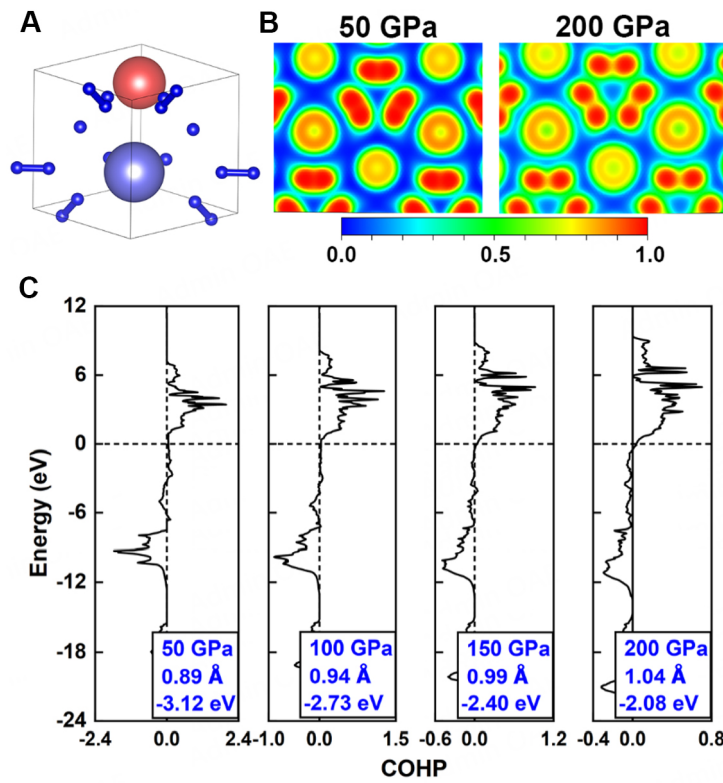


Figure 9. (A) The crystal structure of LaSrH₁₂ at 50 GPa. (B) the ELF of LaSrH₁₂ on the (111) plane at 50 and 200 GPa. (C) The COHP of the nearest distances of H-H for LaSrH₁₂-R3m at 50, 100, 150 and 200 GPa.

Fermi level to decrease to 4.84 states/spin/Ry/f.u. Remarkably, with further pressure elevation, the lowest conduction band at the Γ point accepted electrons, which formed a new electronic pocket at the Fermi level. The Fermi surface had undergone geometric changes, marking Lifshitz transition. As a result, the total electron DOS at the Fermi level increased to 5.55 states/spin/Ry/f.u. at 200 GPa^[66].

We further calculated the phonon band structures, Eliashberg spectral functions $\alpha^2F(\omega)$, and the EPC parameter $\lambda(\omega)$ for LaSrH₁₂ under various pressures [Figure 10]. La and Sr atoms have heavy atomic masses; thus, the low-frequency vibrational modes below 500 cm⁻¹ mainly corresponded to the vibrations of La and

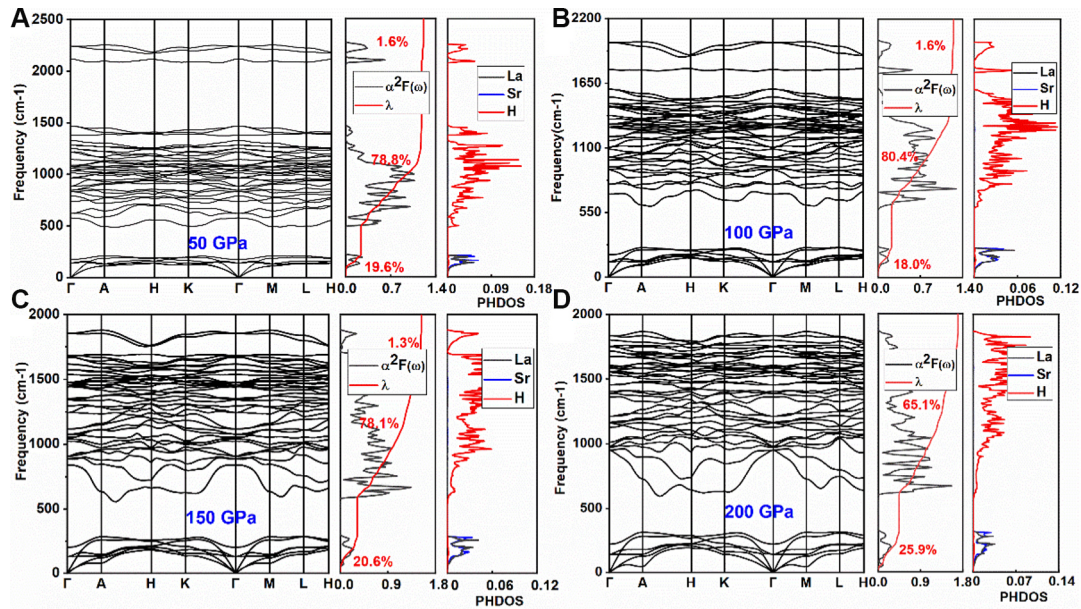


Figure 10. Phonon band structures, Eliashberg spectral function $\alpha^2F(\omega)$ with electron-phonon integral $\lambda(\omega)$, and projected PHDOS of LaSrH₁₂ at (A) 50, (B) 100, (C) 150, and (D) 200 GPa.

Sr atoms with a contribution below 30% of the total λ . The high-frequency regions above 1,700 cm⁻¹ were primarily dominated by the H₂ stretching vibration mode, which accounted for less than 2% of the total λ . The lighter H atoms, which drove the phonon modes in the middle-frequency region, contributed greatly to the EPC and accounted for more than 65% of the total λ . It is noted that the vibration modes in the high-frequency parts are obviously down with rising pressure, and until 200 GPa, there is no clear boundary between the high- and intermediate-frequency regions. The reason is the weakening interaction between H atoms in H₂ units. Besides, we observed that the lowest frequency transverse acoustic phonon mode at points A and M gradually softened with increasing pressure. The emergence of soft modes was beneficial for enhancing the EPC and T_c .

Table 1 lists the critical temperature T_c of LaSrH₁₂ at various pressures obtained by solving the Eliashberg equations using typical Coulomb pseudopotential parameters $\mu^* = 0.1$ and 0.13. The T_c of LaSrH₁₂ is estimated to be within 84–95 K at 50 GPa, almost twice that of LaCaH₁₂ (40.1–46.6 K at 50 GPa)^[67] and it increased nearly linearly with pressure (104–117 K at 100 GPa, 133–146 K at 150 GPa, and 146–160 K at 200 GPa), at an approximate rate (dT_c/dP) of 0.43 K/GPa. To explore the mechanism underlying the positive pressure dependence of T_c , we analyzed the electronic DOS at the Fermi level N_{EF} , logarithmic average frequency ω_{log} , and EPC parameter λ [Figure 11]. According to Equation (1), the T_c is closely related to the EPC constants, λ and ω_{log} . This finding demonstrates that with an increase in pressure, ω_{log} first increased and then decreased, and λ nearly linearly increased with $\lambda = 1.21$ at 50 GPa and $\lambda = 1.70$ at 200 GPa, consistent with the variation trend of T_c . Therefore, the rise in T_c with pressure was mainly due to the increased λ . The EPC parameter λ at low frequency (below 500 cm⁻¹) reached 0.22 at 50 GPa, and increased to 0.45 at 200 GPa, implying a contribution of 57.5% to the increment of total λ . Thus, the softening of low-frequency phonon modes also played an important role in improving the EPC. Hence, the increase in T_c was mainly attributed to the increment in the EPC parameter λ , resulting from the softening of low-frequency phonon modes, the weakening of the interaction between H atoms in H₂ units and Lifshitz transition.

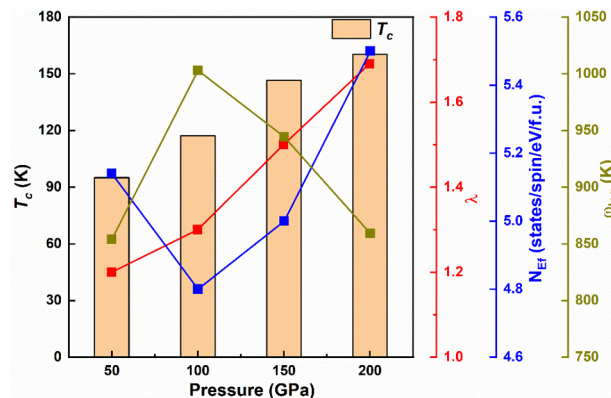


Figure 11. T_c , EPC parameter λ , calculated electronic DOS (N_{EF}) at the Fermi level, and logarithmic average frequencies ω_{log} of LaSrH₁₂-R3m at different pressures.

CONCLUSION

We used evolutionary algorithms to explore the structures of solid La-Sr-H systems at 200 GPa for structural analysis. Thermodynamically stable LaSrH, LaSrH₄, LaSrH₁₂, and LaSr₃H₂₄ and metastable LaSrH₈, LaSr₂H₁₈, and LaSrH₂₁ were identified. However, LaSrH and LaSrH₄ did not exhibit superconductivity. LaSrH₈ became a superconductor near the liquid-nitrogen temperature. LaSrH₂₁ exhibited a high T_c of 211 K, where hydrogen atoms around the La atoms were arranged in H₁₂ rings, which played an important role in attaining a high T_c . LaSrH₁₂, LaSr₂H₁₈, and LaSr₃H₂₄ contained La- and Sr-centered H₂₄ cages and exhibited high T_c of 160, 167, and 169 K at 200 GPa, respectively. Further calculations showed that LaSrH₁₂ can maintain its dynamic stability up to 30 GPa. In addition, the T_c of LaSrH₁₂ increased with pressure at a rate of 0.43 K/GPa, and this finding was mainly attributed to the softening mode and Lifshitz transition.

DECLARATIONS

Authors' contributions

Contributed to the study's conception and design, investigation, original draft writing, editing and review: Chen, L.; Jiang, Q.; Zhang, Z.; Liu, Z.; Huo, Z.; Ma, H.; Guo, S.; Yang, S.; Duan, D.

Availability of data and materials

Not applicable.

Financial support and sponsorship

This work was supported by the National Natural Science Foundation of China (No. 12122405, No. 12274169, and No. 52072188), National Key Research and Development Program of China (No. 2022YFA1402304), Program for Science and Technology Innovation Team in Zhejiang (No. 2021R01004), and Fundamental Research Funds for Central Universities. Parts of calculations were performed at the High Performance Computing Center of Jilin University and TianHe-1(A) at the National Supercomputer Center in Tianjin.

Conflicts of interest

All authors declared that there are no conflicts of interest.

Ethical approval and consent to participate

Not applicable.

Consent for publication

Not applicable.

Copyright

© The Author(s) 2025.

REFERENCES

1. Ashcroft, N. W. Metallic hydrogen: a high-temperature superconductor? *Phys. Rev. Lett.* **1968**, *21*, 1748-9. DOI
2. Bardeen, J.; Cooper, L. N.; Schrieffer, J. R. Microscopic theory of superconductivity. *Phys. Rev.* **1957**, *106*, 162-4. DOI
3. Zhao, W.; Song, H.; Du, M.; et al. Pressure-induced high-temperature superconductivity in ternary Y-Zr-H compounds. *Phys. Chem. Chem. Phys.* **2023**, *25*, 5237-43. DOI
4. Edalati, K.; Bachmaier, A.; Beloshenko, V. A.; et al. Nanomaterials by severe plastic deformation: review of historical developments and recent advances. *Mater. Res. Lett.* **2022**, *10*, 163-256. DOI
5. Kang, S.; Zheng, H.; Liu, T.; et al. A ferromagnetically coupled Fe₄₂ cyanide-bridged nanocage. *Nat. Commun.* **2015**, *6*, 5955. DOI PubMed PMC
6. Dalladay-Simpson, P.; Howie, R. T.; Gregoryanz, E. Evidence for a new phase of dense hydrogen above 325 gigapascals. *Nature* **2016**, *529*, 63-7. DOI PubMed
7. Loubeyre, P.; Occelli, F.; Dumas, P. Synchrotron infrared spectroscopic evidence of the probable transition to metal hydrogen. *Nature* **2020**, *577*, 631-5. DOI PubMed
8. Ashcroft, N. W. Hydrogen dominant metallic alloys: high temperature superconductors? *Phys. Rev. Lett.* **2004**, *92*, 187002. DOI PubMed
9. Du, M.; Zhao, W.; Cui, T.; Duan, D. Compressed superhydrides: the road to room temperature superconductivity. *J. Phys. Condens. Matter.* **2022**, *34*, 173001. DOI PubMed
10. Goncharenko, I.; Eremets, M. I.; Hanfland, M.; et al. Pressure-induced hydrogen-dominant metallic state in aluminum hydride. *Phys. Rev. Lett.* **2008**, *100*, 045504. DOI
11. Eremets, M. I.; Trojan, I. A.; Medvedev, S. A.; Tse, J. S.; Yao, Y. Superconductivity in hydrogen dominant materials: silane. *Science* **2008**, *319*, 1506-9. DOI PubMed
12. Pickard, C. J.; Needs, R. J. Ab initio random structure searching. *J. Phys. Condens. Matter.* **2011**, *23*, 053201. DOI PubMed
13. Wang, Y.; Lv, J.; Zhu, L.; Ma, Y. Crystal structure prediction via particle-swarm optimization. *Phys. Rev. B.* **2010**, *82*, 094116. DOI
14. Wang, Y.; Lv, J.; Zhu, L.; Ma, Y. CALYPSO: a method for crystal structure prediction. *Comput. Phys. Commun.* **2012**, *183*, 2063-70. DOI
15. Gao, H.; Wang, J.; Han, Y.; Sun, J. Enhancing crystal structure prediction by decomposition and evolution schemes based on graph theory. *Fundam. Res.* **2021**, *1*, 466-71. DOI
16. Oganov, A. R.; Glass, C. W. Crystal structure prediction using ab initio evolutionary techniques: principles and applications. *J. Chem. Phys.* **2006**, *124*, 244704. DOI
17. Oganov, A. R.; Lyakhov, A. O.; Valle, M. How evolutionary crystal structure prediction works-and why. *ACC. Chem. Res.* **2011**, *44*, 227-37. DOI PubMed
18. Lyakhov, A. O.; Oganov, A. R.; Stokes, H. T.; Zhu, Q. New developments in evolutionary structure prediction algorithm USPEX. *Comput. Phys. Commun.* **2013**, *184*, 1172-82. DOI
19. Xia, K.; Gao, H.; Liu, C.; et al. A novel superhard tungsten nitride predicted by machine-learning accelerated crystal structure search. *Sci. Bull.* **2018**, *63*, 817-24. DOI
20. Duan, D.; Liu, Y.; Tian, F.; et al. Pressure-induced metallization of dense (H₂S)₂H₂ with high-*T_c* superconductivity. *Sci. Rep.* **2014**, *4*, 6968. DOI PubMed PMC
21. Duan, D.; Huang, X.; Tian, F.; et al. Pressure-induced decomposition of solid hydrogen sulfide. *Phys. Rev. B.* **2015**, *91*, 180502. DOI
22. Drozdov, A. P.; Eremets, M. I.; Troyan, I. A.; Ksenofontov, V.; Shylin, S. I. Conventional superconductivity at 203 kelvin at high pressures in the sulfur hydride system. *Nature* **2015**, *525*, 73-6. DOI PubMed
23. Einaga, M.; Sakata, M.; Ishikawa, T.; et al. Crystal structure of the superconducting phase of sulfur hydride. *Nat. Phys.* **2016**, *12*, 835-8. DOI PubMed PMC
24. Peng, F.; Sun, Y.; Pickard, C. J.; Needs, R. J.; Wu, Q.; Ma, Y. Hydrogen clathrate structures in rare earth hydrides at high pressures: possible route to room-temperature superconductivity. *Phys. Rev. Lett.* **2017**, *119*, 107001. DOI PubMed
25. Liu, H.; Naumov, I. I.; Hoffmann, R.; Ashcroft, N. W.; Hemley, R. J. Potential high-*T_c* superconducting lanthanum and yttrium hydrides at high pressure. *Proc. Natl. Acad. Sci. USA.* **2017**, *114*, 6990-5. DOI PubMed PMC
26. Drozdov, A. P.; Kong, P. P.; Minkov, V. S.; et al. Superconductivity at 250 K in lanthanum hydride under high pressures. *Nature* **2019**, *569*, 528-31. DOI

27. Somayazulu, M.; Ahart, M.; Mishra, A. K.; et al. Evidence for superconductivity above 260 K in lanthanum superhydride at megabar pressures. *Phys. Rev. Lett.* **2019**, *122*, 027001. DOI
28. Hong, F.; Yang, L.; Shan, P.; et al. Superconductivity of lanthanum superhydride investigated using the standard four-probe configuration under high pressures. *Chinese. Phys. Lett.* **2020**, *37*, 107401. DOI
29. Troyan, I. A.; Semenok, D. V.; Kvashnin, A. G.; et al. Anomalous high-temperature superconductivity in YH_6 . *Adv. Mater.* **2021**, *33*, e2006832. DOI
30. Kong, P.; Minkov, V. S.; Kuzovnikov, M. A.; et al. Superconductivity up to 243 K in the yttrium-hydrogen system under high pressure. *Nat. Commun.* **2021**, *12*, 5075. DOI PubMed PMC
31. Ma, L.; Wang, K.; Xie, Y.; et al. High-temperature superconducting phase in clathrate calcium hydride CaH_6 up to 215 K at a pressure of 172 GPa. *Phys. Rev. Lett.* **2022**, *128*, 167001. DOI
32. Jiang, Q.; Zhang, Z.; Song, H.; et al. Ternary superconducting hydrides stabilized via Th and Ce elements at mild pressures. *Fundam. Res.* **2024**, *4*, 550-6. DOI PubMed PMC
33. Errea, I.; Calandra, M.; Pickard, C. J.; et al. Quantum hydrogen-bond symmetrization in the superconducting hydrogen sulfide system. *Nature* **2016**, *532*, 81-4. DOI
34. Errea, I.; Belli, F.; Monacelli, L.; et al. Quantum crystal structure in the 250-kelvin superconducting lanthanum hydride. *Nature* **2020**, *578*, 66-9. DOI
35. Chen, W.; Semenok, D. V.; Huang, X.; et al. High-temperature superconducting phases in cerium superhydride with a T_c up to 115 K below a pressure of 1 megabar. *Phys. Rev. Lett.* **2021**, *127*, 117001. DOI
36. Semenok, D. V.; Kvashnin, A. G.; Ivanova, A. G.; et al. Superconductivity at 161 K in thorium hydride ThH_{10} : synthesis and properties. *Mater. Today*. **2020**, *33*, 36-44. DOI
37. Sun, Y.; Lv, J.; Xie, Y.; Liu, H.; Ma, Y. Route to a superconducting phase above room temperature in electron-doped hydride compounds under high pressure. *Phys. Rev. Lett.* **2019**, *123*, 097001. DOI PubMed
38. Zhang, Z.; Cui, T.; Hutcheon, M. J.; et al. Design principles for high-temperature superconductors with a hydrogen-based alloy backbone at moderate pressure. *Phys. Rev. Lett.* **2022**, *128*, 047001. DOI
39. Song, Y.; Bi, J.; Nakamoto, Y.; et al. Stoichiometric ternary superhydride LaBeH_8 as a new template for high-temperature superconductivity at 110 K under 80 GPa. *Phys. Rev. Lett.* **2023**, *130*, 266001. DOI
40. Heil, C.; di, C. S.; Bachelet, G. B.; Boeri, L. Superconductivity in sodalite-like yttrium hydride clathrates. *Phys. Rev. B.* **2019**, *99*, 220502. DOI
41. Xie, H.; Duan, D.; Shao, Z.; et al. High-temperature superconductivity in ternary clathrate CaYH_{12} under high pressures. *J. Phys. Condens. Matter.* **2019**, *31*, 245404. DOI
42. Liang, X.; Bergara, A.; Wang, L.; et al. Potential high- T_c superconductivity in CaYH_{12} under pressure. *Phys. Rev. B.* **2019**, *99*, 100505. DOI
43. Zhao, W.; Duan, D.; Du, M.; et al. Pressure-induced high- T_c superconductivity in the ternary clathrate system Y-Ca-H. *Phys. Rev. B.* **2022**, *106*, 014521. DOI
44. Chen, W.; Huang, X.; Semenok, D. V.; et al. Enhancement of superconducting properties in the La-Ce-H system at moderate pressures. *Nat. Commun.* **2023**, *14*, 2660. DOI PubMed PMC
45. Bi, J.; Nakamoto, Y.; Zhang, P.; et al. Giant enhancement of superconducting critical temperature in substitutional alloy $(\text{La,Ce})\text{H}_9$. *Nat. Commun.* **2022**, *13*, 5952. DOI PubMed PMC
46. Semenok, D. V.; Troyan, I. A.; Ivanova, A. G.; et al. Superconductivity at 253 K in lanthanum-yttrium ternary hydrides. *Mater. Today*. **2021**, *48*, 18-28. DOI
47. Ma, T.; Zhang, Z.; Du, M.; et al. High-throughput calculation for superconductivity of sodalite-like clathrate ternary hydrides MXH_{12} at high pressure. *Mater. Today. Phys.* **2023**, *38*, 101233. DOI
48. Hooper, J.; Terpstra, T.; Shamp, A.; Zurek, E. Composition and constitution of compressed strontium polyhydrides. *J. Phys. Chem. C.* **2014**, *118*, 6433-47. DOI
49. Wang, Y.; Wang, H.; Tse, J. S.; Iitaka, T.; Ma, Y. Structural morphologies of high-pressure polymorphs of strontium hydrides. *Phys. Chem. Chem. Phys.* **2015**, *17*, 19379-85. DOI
50. Semenok, D. V.; Kruglov, I. A.; Savkin, I. A.; Kvashnin, A. G.; Oganov, A. R. On distribution of superconductivity in metal hydrides. *Curr. Opin. Solid. State. Mater. Sci.* **2020**, *24*, 100808. DOI
51. Tanaka, K.; Tse, J. S.; Liu, H. Electron-phonon coupling mechanisms for hydrogen-rich metals at high pressure. *Phys. Rev. B.* **2017**, *96*, 100502. DOI
52. Semenok, D. V.; Chen, W.; Huang, X.; et al. Sr-doped superionic hydrogen glass: synthesis and properties of SrH_{22} . *Adv. Mater.* **2022**, *34*, e2200924. DOI
53. Chen, Y.; Liu, Z.; Lin, Z.; et al. High T_c superconductivity in layered hydrides XH_{15} ($\text{X} = \text{Ca}, \text{Sr}, \text{Y}, \text{La}$) under high pressures. *Front. Phys.* **2022**, *17*, 63502. DOI
54. Kresse, G.; Furthmüller, J. Efficient iterative schemes for ab initio total-energy calculations using a plane-wave basis set. *Phys. Rev. B. Condens. Matter.* **1996**, *54*, 11169-86. DOI PubMed
55. Perdew, J. P.; Burke, K.; Ernzerhof, M. Generalized gradient approximation made simple. *Phys. Rev. Lett.* **1996**, *77*, 3865-8. DOI PubMed
56. Perdew, J. P.; Wang, Y. Pair-distribution function and its coupling-constant average for the spin-polarized electron gas. *Phys. Rev. B.*

- Condens. Matter.* **1992**, *46*, 12947-54. DOI PubMed
57. Blöchl, P. E. Projector augmented-wave method. *Phys. Rev. B. Condens. Matter.* **1994**, *50*, 17953-79. DOI PubMed
58. Maintz, S.; Deringer, V. L.; Tchougréeff, A. L.; Dronskowski, R. LOBSTER: a tool to extract chemical bonding from plane-wave based DFT. *J. Comput. Chem.* **2016**, *37*, 1030-5. DOI PubMed PMC
59. Togo, A.; Oba, F.; Tanaka, I. First-principles calculations of the ferroelastic transition between rutile-type and CaCl_2 -type SiO_2 at high pressures. *Phys. Rev. B.* **2008**, *78*, 134106. DOI
60. Giannozzi, P.; Baroni, S.; Bonini, N.; et al. QUANTUM ESPRESSO: a modular and open-source software project for quantum simulations of materials. *J. Phys. Condens. Matter.* **2009**, *21*, 395502. DOI
61. Vanderbilt, D. Soft self-consistent pseudopotentials in a generalized eigenvalue formalism. *Phys. Rev. B. Condens. Matter.* **1990**, *41*, 7892-5. DOI
62. Appel, J. Transition temperature of d-f-band superconductors. *Phys. Rev. B.* **1973**, *8*, 1079-87. DOI
63. Wu, Y.; Lazic, P.; Hautier, G.; Persson, K.; Ceder, G. First principles high throughput screening of oxynitrides for water-splitting photocatalysts. *Energy. Environ. Sci.* **2013**, *6*, 157-68. DOI
64. Hinuma, Y.; Hatakeyama, T.; Kumagai, Y.; et al. Discovery of earth-abundant nitride semiconductors by computational screening and high-pressure synthesis. *Nat. Commun.* **2016**, *7*, 11962. DOI PubMed PMC
65. Song, H.; Zhang, Z.; Cui, T.; Pickard, C. J.; Kresin, V. Z.; Duan, D. High T_c superconductivity in heavy rare earth hydrides. *Chinese. Phys. Lett.* **2021**, *38*, 107401. DOI
66. Lifshitz, I. M. Anomalies of electron characteristics in the high pressure region. 1960. Available from: <https://www.osti.gov/biblio/4173345> [Last accessed on 15 Jul 2024].
67. Yang, K.; Sun, H.; Chen, H.; Chen, L.; Li, B.; Lu, W. Stable structures and superconducting properties of Ca-La-H compounds under pressure. *J. Phys. Condens. Matter.* **2022**, *34*, 355401. DOI